Please cite this article in press as: Ebady et al., Biomechanics of *Borrelia burgdorferi* Vascular Interactions, Cell Reports (2016), http://dx.doi.org/10.1016/j.celrep.2016.08.013

Cell Reports
Article



# Biomechanics of *Borrelia burgdorferi* Vascular Interactions

Rhodaba Ebady,[1] Alexandra F. Niddam,[1] Anna E. Boczula,[1] Yae Ram Kim,[1] Nupur Gupta,[1] Tian Tian Tang,[1] Tanya Odisho,[1] Hui Zhi,[4] Craig A. Simmons,[1,3] Jon T. Skare,[4] and Tara J. Moriarty[1,2,5,*]
[1]Matrix Dynamics Group, Faculty of Dentistry
[2]Department of Laboratory Medicine & Pathobiology, Faculty of Medicine
University of Toronto, 150 College Street, #241 Toronto, ON M5S 3E2, Canada
[3]Department of Mechanical & Industrial Engineering, Faculty of Applied Science & Engineering, University of Toronto, 661 University Avenue, 14th floor, Toronto, ON M5G 1M1, Canada
[4]Department of Microbial Pathogenesis & Immunology, Texas A&M Health Science Center, 8447 State Highway 47, MREB #3107, Bryan, TX 77807, USA
[5]Lead Contact
*Correspondence: tara.moriarty@utoronto.ca
http://dx.doi.org/10.1016/j.celrep.2016.08.013

## SUMMARY

**Systemic dissemination of microbes is critical for progression of many infectious diseases and is associated with most mortality due to bacterial infection. The physical mechanisms mediating a key dissemination step, bacterial association with vascular endothelia in blood vessels, remain unknown. Here, we show that endothelial interactions of the Lyme disease spirochete *Borrelia burgdorferi* under physiological shear stress mechanistically resemble selectin-dependent leukocyte rolling. Specifically, these interactions are mediated by transfer of mechanical load along a series of adhesion complexes and are stabilized by tethers and catch bond properties of the bacterial adhesin BBK32. Furthermore, we found that the forces imposed on adhesive bonds under flow may be small enough to permit active migration driven by bacterial flagellar motors. These findings provide insight into the biomechanics of bacterial-vascular interactions and demonstrate that disseminating bacteria and circulating host immune cells share widely conserved mechanisms for interacting with endothelia under physiological shear stress.**

## INTRODUCTION

Systemic dissemination of microbial pathogens is a critical step in infectious disease progression and is associated with most mortality due to bacterial infections. A key event in dissemination is pathogen adhesion to vascular endothelium and transmigration from blood into extravascular tissues (extravasation), which is mediated by bacterial cell-surface adhesion proteins (adhesins) and cognate host ligands (receptors) (Lemichez et al., 2010). This interaction must overcome shear stress caused by blood flow, which subjects adhesin-receptor complexes to tension, a form of mechanical load (Persat et al., 2015; Sokurenko et al., 2008). The initial braking steps of vascular interactions are critical because they permit microbes to reduce velocity and move along vessel walls until extravasation sites are reached.

Cell association with endothelial surfaces is especially difficult in the constantly changing shear stress environment of the vasculature. The conventional "slip" bonds formed by many receptor-ligand complexes in static environments break at exponential rates when subjected to small force increases constantly encountered in the vasculature (Park et al., 2002). For circulating host cells such as leukocytes rolling along surfaces of postcapillary venules (PCVs), the first steps of vascular interaction require mechanically specialized, force-strengthened catch or flex bonds, which confer dynamic, tensile strength to interactions under shear stress (Fiore et al., 2014; Kim et al., 2010; Marshall et al., 2003; Sarangapani et al., 2004; Sokurenko et al., 2008). Catch bonds stabilize molecular interactions over extended force ranges, causing adhesion complexes to become longer lived and dissociate more slowly above specific shear stress and force thresholds (Sokurenko et al., 2008).

Interaction of circulating cells with endothelia is not stabilized by catch bonds alone, but also by tension-responsive, stretchable cellular and extracellular structures physically associated with adhesion complexes. Stretching these structures "shares" or distributes the force imposed on adhesion complexes, reducing the mechanical load they bear and increasing bond lifetime. For example, leukocyte rolling is stabilized by elastic membrane tethers that anchor cells to endothelial surfaces and prevent their full detachment (Ramachandran et al., 2004; Sundd et al., 2011). Tethers and catch bonds can independently stabilize leukocyte rolling under lower shear stress conditions but act together to strengthen interactions at higher shear stresses. Bacteria circulating in the bloodstream face the same mechanical barriers to vascular adhesion and extravasation as circulating host cells, but the physical mechanisms permitting their adhesion to vascular surfaces under physiological shear stress are largely unknown.

Please cite this article in press as: Ebady et al., Biomechanics of *Borrelia burgdorferi* Vascular Interactions, Cell Reports (2016), http://dx.doi.org/10.1016/j.celrep.2016.08.013

Our understanding of the mechanics by which bacteria adhere to non-endothelial surfaces under force and flow has advanced considerably in recent years, primarily for bacteria that tether to surfaces via extendible, shock-absorbing and force-distributing surface appendages such as pili and fimbriae (Beaussart et al., 2014; Persat et al., 2015; Utada et al., 2014). However, bacterial adhesion to endothelia via such structures requires transient reductions in flow and stabilization by host filopodia that cover adherent bacteria (Mairey et al., 2006; Mikaty et al., 2009). Only two adhesins supporting bacterial interactions with endothelia under physiological shear stress have been identified, and neither associates with fimbriae or pili (Claes et al., 2014; Norman et al., 2008). One of these is BBK32, a lipoprotein of the Lyme disease spirochete *Borrelia burgdorferi*. *B. burgdorferi* is a long, thin (<0.3 × 10–20 μm), highly motile, invasive bacterium with a planar sine-wave morphology, internal periplasmic flagella, and no external appendages that could tether bacteria to surfaces under flow (Charon et al., 2012). Vascular dissemination is central to infection by *B. burgdorferi* and other spirochetes, including those which cause syphilis, relapsing fever, and leptospirosis (Wormser, 2006).

*B. burgdorferi* extravasate extremely rapidly from PCVs (<150 ms to penetrate endothelial lining) in a process that does not require bacterial stationary adhesion and is initiated by two mechanistically distinct interaction types, tethering and dragging, which move faster and slower than 100 μm/s, respectively, along PCV surfaces (Moriarty et al., 2008). BBK32 is required for early dissemination and full *B. burgdorferi* infectivity and mediates both tethering and dragging in PCVs, via its fibronectin (Fn)- and glycosaminoglycan (GAG)-binding sequences (Hyde et al., 2011; Lin et al., 2015; Moriarty et al., 2012; Norman et al., 2008; Seshu et al., 2006). Genetic *bbk32* disruption does not eliminate *B. burgdorferi* tethering and dragging, implying that it is not the only adhesin that can mediate these interactions (Moriarty et al., 2012). However, other adhesins supporting tethering and dragging have not yet been identified. The endothelial receptors targeted by disseminating *B. burgdorferi* are also unknown.

To understand bacterial dissemination, it is critical to understand the physical mechanisms of bacterial-endothelial interactions under physiological shear stress not only at a molecular level, but in living cells. We studied the physical mechanisms supporting *B. burgdorferi* interactions with endothelia in real time in flow chambers under controlled shear stress and in PCVs of live mice, using particle tracking methods. These studies provided insight into physical mechanisms of bacterial-endothelial interactions and revealed remarkable similarities in the mechanisms by which bacteria and leukocytes interact with and move over endothelial surfaces, including dependence on tethers and catch bonds.

## RESULTS AND DISCUSSION

### Development of a Flow Chamber System to Study *B. burgdorferi*-Endothelial Interaction Mechanisms under Controlled Physiological Shear Stress

Investigating bacterial-endothelial interaction biomechanics requires tools such as flow chambers for studying interactions in a force-controlled environment, and high temporal resolution tracking of interaction kinetics. Therefore, we developed a flow chamber system and real-time tracking methods enabling fluorescence microscopy analysis of *B. burgdorferi* interactions with primary human endothelia under controlled shear stress.

The flow chamber system was developed and validated by comparing interactions visualized in dermal PCVs of live mice by real-time intravital microscopy (IVM: in vivo live cell imaging) with interactions visualized in flow chambers. Validation was performed using two genetically distinct BBK32-producing infectious *B. burgdorferi* strains (GCB966, GCB726), which interact with PCVs with different efficiencies. In addition, we tested a non-infectious negative control strain (GCB706) that does not encode many adhesins expressed by infectious strains, including BBK32, and interacts with PCVs less than GCB726 and GCB966 (Table S1). We tested the effects of different experimental conditions on interaction abundance, to identify conditions that maximized numbers of slow-moving (dragging) interactions for infectious bacteria (Figures S1A–S1F). Optimal dragging was observed for infectious bacteria cultivated in mouse blood, and primary human umbilical vein cells (HUVECs) grown to 2 days post-confluence, with addition of 10% serum to perfusion medium.

Major qualitative features previously reported for *B. burgdorferi* PCV interactions were recapitulated in flow chambers (Moriarty et al., 2008, 2012; Norman et al., 2008). *B. burgdorferi* interacted with endothelia in flow chambers by tethering, dragging and stationary adhesion, and tethering and dragging occurred at both endothelial junctions and extrajunctional apical surfaces (Movies S1, S2, S3, and S4). Flow chamber interactions were inhibited by antibodies to Fn (Figure S1G) and by competition with heparin (Figure S1H), indicating that host molecules mediating interactions in the flow chamber system and PCVs were similar.

Interaction abundance and relative differences in interaction numbers among strains were also similar in vitro and in PCVs. For these experiments, we manually counted tethering and dragging interactions in flow chambers at 0.5, 0.75, 1, 1.25, 1.75, 2, 2.25, 2.75, 3 dyn/cm$^2$, which corresponds to shear stress range in PCVs (Sundd et al., 2011). We then compared global mean values for combined shear stresses to interaction numbers measured in PCVs (Figure 1A). Tethering was greater in vitro for all strains due to more efficient detection of fast-moving bacteria in flow chambers, but dragging numbers in vitro and in PCVs were similar. Relative differences in interaction numbers among strains were also similar in PCVs and in vitro, in the order GCB966 > GCB726 > GCB706 (Figure 1A). Taken together, these data showed that the flow chamber system recapitulated interaction conditions and properties found in PCVs.

### Development of Tracking Methods to Study *B. burgdorferi*-Endothelial Interaction Biomechanics

We next developed particle tracking methods to study the tracks of individual bacterial interactions in time-lapse footage from flow chamber and IVM experiments (Figures 1B–1D). Detailed description of these methods and their validation is provided in Supplemental Experimental Procedures. To ensure that we studied the slowest, most physiologically relevant interactions,

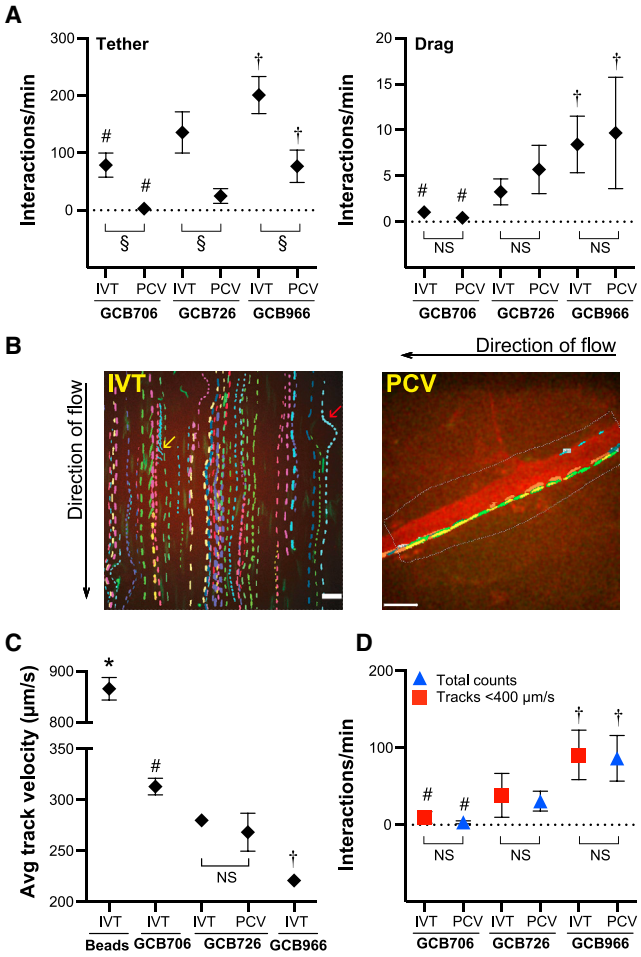


**Figure 1. Flow Chamber Model System and Particle Tracking Methods Developed to Study *B. burgdorferi*-Endothelial Interactions under Controlled Shear Stress**

Comparison of numbers and velocities of bacteria interacting with PCVs in live mice and human endothelia IVT, captured by spinning disk confocal microscopy and measured by manual counting and particle tracking of interaction trajectories (tracks). To replicate variable shear stress conditions in PCVs (ranging from 0.5 to 3 dyn/cm$^2$), IVT experiments were conducted at each of 0.5, 0.75, 1, 1.25, 1.75, 2, 2.25, 2.75, and 3 dyn/cm$^2$. Shown are global means interaction numbers and velocities from 0.5 to 3 dyn/cm$^2$. *B. burgdorferi* strains: adhesion-attenuated non-infectious *bbk32*-null negative control (GCB706), adhesive infectious genetically distinct BBK32-expressing positive-control strains differing in adhesion efficiency (GCB726, GCB966).

(A) Numbers of manually counted tethering and dragging interactions. Tethering but not dragging is lower in PCVs than IVT. Tethering and dragging differ among strains IVT and in PCVs.

(B) Sample time-lapse projections of tracks for individual bacteria. Each track is shown in a different color. Scale bars for IVT, 13 μm; PCV, 32 μm). Endothelial counterstain (red): plasma membrane dye (IVT), AlexaFluor 555-PECAM-1 antibody (PCV). Yellow and red arrows: *B. burgdorferi* interacting by one end only (yellow) and moving along edge of endothelial nucleus projecting above imaging plane (red). Black arrows: flow direction.

(C) Track velocities of bacteria and non-adhesive negative control beads. Beads move faster than bacteria. Velocities differ among strains, but not IVT versus PCVs.

(D) Total interactions counted in PCVs (tethering + dragging) are similar to track numbers IVT with velocities <400 μm/s. Strain-specific differences in interaction numbers in PCVs are similar to strain-specific track numbers IVT.

we analyzed tracks with velocities <400 μm/s, which is less than half the velocity of negative control beads in vitro (Figure 1C) and in PCVs (Moriarty et al., 2008). Tracking captured all types of bacterial movement seen in PCVs, including tethering, dragging, and stationary adhesion, as well as bacteria interacting with endothelia while moving parallel to flow and rotating bacteria interacting by one end only (Figure 1B) (Moriarty et al., 2008). Some tracks also followed the lateral contours of endothelial nuclei projecting above the imaging plane (Figure 1B), confirming that tracked bacteria were interacting with endothelial surfaces.

To determine whether tracking captured the same interaction populations in flow chambers and in PCVs, we compared track numbers and velocities of interactions captured from 0.5–3 dyn/cm$^2$ in flow chambers to track numbers and velocities captured in PCVs. Track velocities (Figure 1C) and numbers (Figure 1D) were similar in vitro and in PCVs. Furthermore, we found that bacterial strains that interacted most abundantly with endothelia in flow chambers and PCVs (Figure 1D) were those with the slowest velocities (Figure 1C). Thus, tracking identified the same populations in vitro and in PCVs and accurately captured strain-specific differences in interaction properties.

### *B. burgdorferi*-*Endothelial Interaction Trajectories Consist of Repeating Interaction Cycles*

To study the physical mechanisms mediating bacterial-endothelial interactions under shear stress, we first examined changes in instantaneous bacterial velocity over time (Figure 2A). To our surprise, these profiles were remarkably similar to the "jerky" instantaneous velocity profiles of leukocytes rolling along endothelia under similar shear stresses (Alon et al., 1997). This prompted us to examine whether *B. burgdorferi*-endothelial interactions shared physical mechanisms important for leukocyte rolling.

Rolling leukocytes advance along endothelia without fully detaching via series of repeating deceleration and acceleration cycles in which mechanical force is first loaded onto a single receptor-ligand complex (deceleration) and then transferred to a new complex as the first bond reaches its maximal load and breaks (acceleration) (Alon et al., 1997; Sundd et al., 2011). Load transfer along a series of successively formed and broken bonds permits cells to move over surfaces at stable overall velocity since acceleration and deceleration within each interaction cycle are balanced and net acceleration is zero. The ability to sustain stable velocities without detaching or stably arresting is critical for leukocyte sampling of the environment and directed migration to extravasation sites and would likely facilitate bacterial-endothelial interactions and dissemination.

To determine whether physical mechanisms of leukocyte rolling were shared by *B. burgdorferi* interacting with endothelia, we

In this and all figures: IVT, in vitro: flow chamber; PCV, dermal postcapillary venules. Summary values: ±95% CI. Replicates: n ≥ 27 replicates/strain and bead controls (IVT: three or more independent replicates/shear stress); ≥16 mice/strain (PCV). Table S2: numbers of tracks and interactions analyzed in each experiment. Statistics: two-way ANOVA, Holm-Sidak post-test. Table S1: bacterial strain details. *, #, †$p < 0.05$ versus all groups for beads, GCB706, GCB966, respectively, within the same experimental system (PCVs or IVT). For IVT versus PCVs, § and NS indicate $p < 0.05$, >0.05, respectively. See also Figure S1.

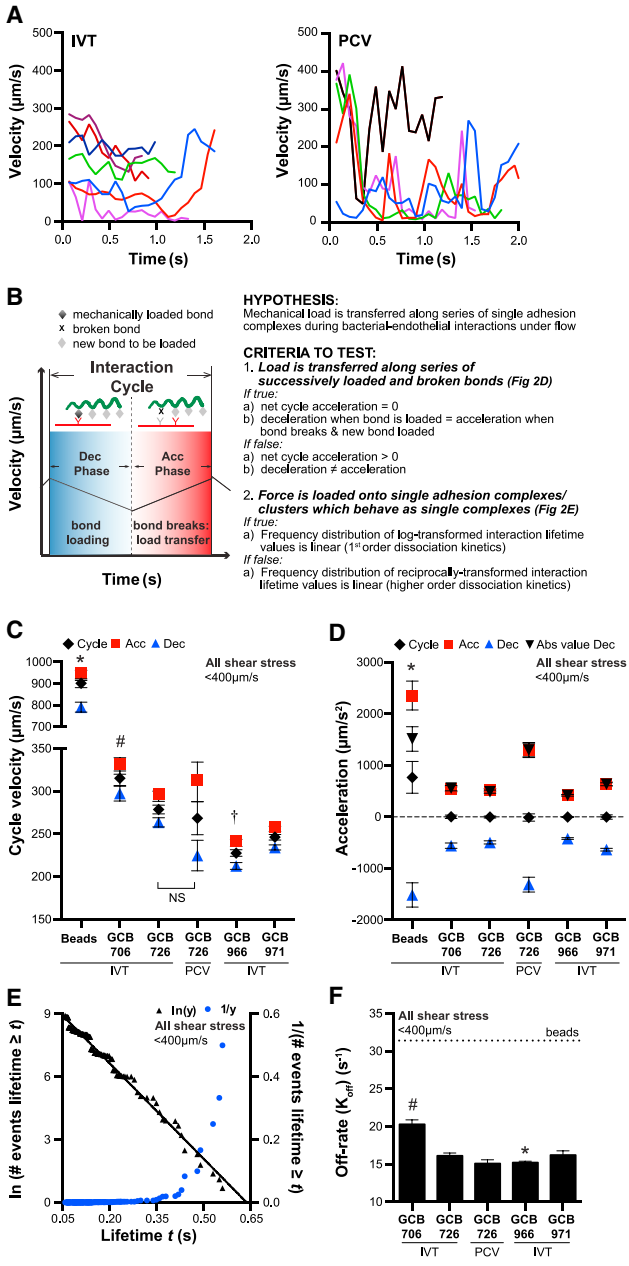


**Figure 2. Transfer of Load along Series of Adhesion Complexes during *B. burgdorferi*-Endothelial Interactions at Postcapillary Venule Shear Stress Range**

(A and B) Sample instantaneous velocity versus track duration kymographs for *B. burgdorferi*-endothelial interactions (A). The "jerky" pattern resembles instantaneous velocity kymographs of leukocytes rolling on PCV surfaces, which result from repetition of an interaction cycle comprising bond-loading (deceleration: Dec) and bond-unloading (acceleration: Acc) phases (B). At typical PCV shear stress (1 dyn/cm$^2$), leukocytes roll over endothelia without net acceleration or deceleration by transferring mechanical load along series of single molecule adhesion complexes formed by one leukocyte and one endothelial receptor.

(C and D) Velocities and acceleration magnitudes for bacterial interaction cycles and constituent acceleration and deceleration phases. Cycle velocities (C) and track velocities (Figure 1C) are similar ($p > 0.05$) for all strains, implying that cycles are the basic repeating unit of tracks. (D) Net cycle acceleration values of 0 and identical acceleration and deceleration magnitudes within each cycle ($p > 0.05$: compare Acc to Abs value Dec, absolute value of deceleration) show that bacteria move along endothelia without net acceleration or deceleration by transferring load along adhesion complexes series.

(E and F) First-order dissociation kinetics of interaction lifetimes showing that each interaction is mediated by a single adhesion complex, or by tightly clustered and coordinated complexes that behave as a single bond (shown: GCB966) (E). (F) Interaction dissociation rates. Beads: threshold at which interactions dissociate as fast as non-adherent beads, i.e., are unstable.

*, #, †$p < 0.05$ versus all groups for beads, GCB706, GCB966, respectively (C and D: cycle values only). Strains: adhesion-attenuated *bbk32*-null GCB706, adhesive BBK32-expressing GCB726 and GCB966, *bbk32*-null GCB966-derived isogenic strain (GCB971). See also Figures S1C and S2.

first investigated whether tracks consisted of repeating interaction cycles by identifying successive time points within each track where bacteria were accelerating and decelerating (Figure 2B: acceleration and deceleration phases). To study the contributions of a specific adhesin, BBK32, to interactions we also examined the properties of a well-characterized isogenic GCB966 derivative in which the *bbk32* gene is insertionally inactivated (GCB971: Figure S1C; Table S1), which interacts with PCVs and disseminates to tissues less than GCB966 (Hyde et al., 2011; Moriarty et al., 2012).

As shown in Figure S2A, acceleration and deceleration frequencies for bacteria were less than for control beads (beads: 31.40 ± 1.04 Hz), indicating that they were due to bacterial-interaction-specific properties, and not to random measurement variation. Velocities measured over cycles comprising one acceleration and deceleration phase—i.e., cycle velocity—differed among strains, in the order GCB966 < GCB971 < GCB726 < GCB706 (Figure 2C). Within the same strain, cycle velocities were the same as track velocities calculated by measuring total bacterial displacement over total trajectory duration ($p > 0.79$; Figure 1C). This implied that the physical properties of whole tracks were averages of the properties of individual interaction cycles within tracks. Thus, the physical properties of interactions could be studied by examining individual interaction cycles.

## *B. burgdorferi* Moves at Stable Velocity along Endothelial Surfaces without Detaching by Transferring Mechanical Load along a Series of Adhesion Complexes

To determine whether, like rolling leukocytes, bacteria moved over endothelia at stable velocities consistent with load transfer along series of adhesion complexes (Figures 2B and 2D), we measured net acceleration over each interaction cycle. Net cycle acceleration for all bacterial strains over successive deceleration and acceleration phases was zero, both in vitro and in PCVs (average: −1.269 ± 3.673 μm/s$^2$; no significant difference among strains), and deceleration and acceleration magnitudes within successive phases were the same within strains ($p > 0.05$; Figure 2D: acceleration versus deceleration absolute values). This indicated that each round of deceleration and acceleration corresponded to an interaction cycle in which adhesion complexes were, respectively, force loaded and unloaded. By contrast, beads exhibited large net positive acceleration (Figure 2D: 767 ± 158 μm/s$^2$), as would be expected for unstable/detaching interactions. Thus, bacteria moved over endothelia by stably transferring load along a series of adhesion complexes.

### *Mechanical Load Is Borne by a Single Adhesion Complex during Each Interaction or by Tightly Coordinated Complexes that Behave as a Single Bond*

To determine the number of load-bearing adhesion complexes mediating interactions, we examined the frequency distributions of log- and reciprocally transformed deceleration phase lifetimes (duration of individual deceleration phases) (Figures 2B and 2E), as reported previously (Alon et al., 1995). Linear frequency distribution of log-transformed lifetimes implies that interactions exhibit first-order dissociation kinetics and are mediated by single adhesion complexes or tightly clustered and physically coordinated complexes that are loaded and break with the kinetics of a single bond (Alon et al., 1995). By contrast, if interactions are mediated by multiple non-clustered complexes, frequency distributions of reciprocally transformed lifetime data are linear.

GCB966 lifetimes pooled from all tracks with velocities <400 μm/s at 0.5–3 dyn/cm$^2$ exhibited first-order dissociation kinetics (Figure 2E; $R^2 = 0.99$), as did all other bacterial strains in vitro and in PCVs (Figures S2B and S2C; $R^2 > 0.95$). Comparison of interaction dissociation rates, estimated from negative slopes of log-transformed lifetime frequency data (Alon et al., 1995; Sarangapani et al., 2004), showed that GCB966 interactions dissociated more slowly than interactions for other strains (Figure 2F; GCB966 < GCB726 ≈ GCB971 < GCB706). Therefore, bacteria moved along endothelia at constant velocity, without fully detaching, by transferring mechanical load along a series of single adhesion complexes or tightly clustered complexes that behaved as a single complex. Collectively, these data showed that, despite their obvious differences in phylogeny, form, and function, the basic physical mechanisms supporting interaction of leukocytes and *B. burgdorferi* with endothelia and PCV surfaces are unexpectedly conserved.

### *B. burgdorferi* Rotates from an Edge-On to Flat Orientation during Each Interaction

Despite sharing load-transfer mechanisms, leukocytes are deformable spheres that roll along endothelia (Sundd et al., 2011), whereas *B. burgdorferi* are longer and thinner than leukocytes, have a flat, slightly helical sine-wave morphology (Figure 3A) (Charon et al., 2012), and primarily move along endothelia parallel to flow rather than by rolling or flipping end over end (Figure 1B) (Moriarty et al., 2008). To understand how bacteria moved during interactions with endothelia, we examined changes in their conformation in three dimensions. Conformational changes were measured during deceleration for interactions with velocities <300 μm/s, since faster interactions destabilized as shear stress increased (Figure S3A).

First, we determined whether bacteria were deformed under flow, by examining the length: diameter ratios of bacteria under flow to bacterial length: diameter ratios under no-flow (static) conditions (Figure 3B). All strains, with the exception of adhesion-attenuated GCB706, exhibited lengthwise compression during interactions with endothelia under flow (Figure 3B). Although the measured ratios of BBK32-producing GCB966 and *bbk32*-null GCB971 did not differ under static conditions (Figure S3B), under flow GCB966 was more compressed than GCB971 (Figure 3B), implying that differences in adhesive properties affected bacterial conformation. Bacterial compression was also absent at low shear stress (0.5 dyn/cm$^2$: Figure S3D), but at shear stresses >0.5 dyn/cm$^2$ bacteria assumed a compressed conformation at interaction outset, which relaxed as they displaced (Figure 3C). Similarly, interaction displacement increased as bacteria lengthened and relaxed (Figures 3D and 3E), confirming that bacteria began interactions in a compressed conformation but relaxed as interactions progressed.

At interaction outset, bacterial surface area visualized in the imaging focal plane, which was parallel to the endothelial surface, was also smaller than would be expected if bacteria were lying flat on surfaces, but increased as interactions progressed ($p < 0.05$). This suggested that bacterial compression at interaction outset was not due to compression in the xy focal plane of the endothelial surface, but to vertical projection of parts of bacteria above this surface.

To determine how high bacteria projected above endothelial surfaces under flow, we first estimated the average cylindrical volume of individual bacteria for each strain, as described in Figure S3C, using strain-specific volumes calculated from cell lengths measured under no-flow conditions (Figure S3B), and known constants for the half-amplitude of the *B. burgdorferi* sine wave (555 nm) and radius of the cell body (165 nm) (Goldstein et al., 1996). As described in Figure S3C, we then calculated the radius of the height of bacteria projecting above endothelial surfaces during interactions ($r$), using strain-specific volumes, and bacterial length and diameter values measured at each time point. Due to its flat sine-wave morphology, *B. burgdorferi* can lie flat on or be oriented with the edge of its sine wave perpendicular to surfaces (edge-on orientation). To distinguish between these orientations, we compared $r$ values under flow to known values for *B. burgdorferi* cell thickness (flat-on height) and wave amplitude (edge-on height) previously measured by electron microscopy (Goldstein et al., 1996).

All strains except adhesion-attenuated GCB706 exhibited a non-flat orientation during interactions under flow, and $r$ values for GCB966 were higher than for GCB971 (Figure 3F). Therefore, more adhesive bacteria projected higher above endothelial surfaces. Spirochetes were also oriented flat against surfaces at 0.5 dyn/cm$^2$ (Figure S3E), but at higher shear stresses bacteria began interactions with endothelia in an edge-on orientation and rotated to a flat orientation as they displaced (Figure 3G). Similarly, projection above surfaces declined as bacteria lengthened (Figure 3H). These data indicated that bacteria rotated from an edge-on to flat orientation during each interaction.

### Bacterial Rotation during Each Interaction Orients Adhesion Sites at Successive Sine-Wave Peaks toward Endothelial Surfaces, Facilitating Stepwise Displacement

Bacterial rotation into the focal plane at the endothelial surface influences the position of the cell centroid measured by tracking algorithms, and hence bacterial displacement measurements. To address this possibly confounding issue, and estimate how much of bacterial displacement during interactions was due to conformational change, we calculated the percentage of total interaction displacement that was due to net change in bacterial length (Figure 3I). Since a substantial part of bacterial displacement was also due to tether extension (see below), we

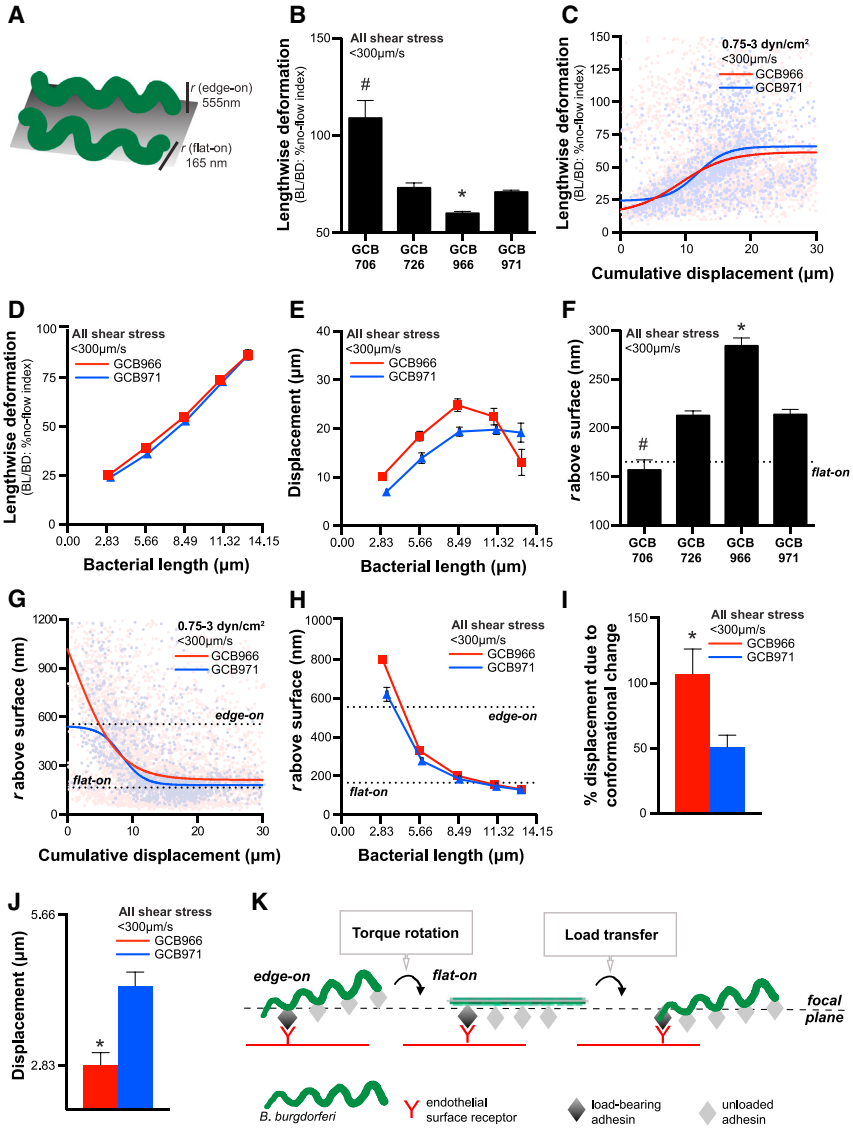


**Figure 3. *B. burgdorferi* Conformation during Endothelial Interactions under Physiological Shear Stress**

(A) Schematic: vertical projection (*r*: radius) of the *B. burgdorferi* planar sine wave when it is oriented flat on or perpendicular to surfaces (edge-on). In (F)–(H), these values are shown as dotted lines.

(B–E) Lengthwise deformation of adhesion-attenuated GCB706 and other strains during interactions (B). Lengthwise deformation is the ratio of bacterial length: diameter and is expressed as a percentage of strain-specific ratios measured under no-flow conditions. Bacterial decompression/relaxation with increasing interaction displacement (C) and bacterial length (D). (E) Increased interaction displacement with increased bacterial length. In (D) and (E), average lengthwise deformation and displacement were measured for interactions binned by bacterial length.

(F–H) Radius of vertical bacterial projection above endothelial surfaces during interactions (F). Bacterial rotation to a flat orientation with increasing interaction displacement (G) and bacterial length (H).

(I and J) During each interaction, BBK32-expressing GCB966 *B. burgdorferi* advances in stepwise increments of approximately one wavelength of the bacterial sine wave (2.83 μm) (J), due entirely to bacterial conformational change (I). *bbk32*-null GCB971 displaces by both conformational change-dependent and -independent mechanisms. Interactions analyzed: untethered bacteria (–T: see Figure 5).

(K) Model: *B. burgdorferi*-endothelial interactions under shear stress are initiated in an edge-on orientation. Bacteria then appear to relax and lengthen as torque due to fluid flow or possibly bacterial motility rotates the cell into a flat orientation with respect to the endothelial surface. This rotation brings unloaded adhesion complexes at the next sine-wave peak into closer contact with the endothelial surface, facilitating transfer of mechanical load from one complex to the next. Centroid positions of individual bacteria and the imaging focal plane are shown to illustrate how bacteria can appear to displace as they rotate.

#, *$p < 0.05$ versus all groups for GCB706, GCB966, respectively. Strains: adhesion-attenuated *bbk32*-null GCB706, adhesive BBK32-expressing GCB726 and GCB966, *bbk32*-null GCB966-derived GCB971. See also Figure S3.

performed these calculations only for bacteria that traveled less than their length under flow and were not anchored to endothelia by tethers (see below: –T interactions).

This analysis revealed that for BBK32-expressing GCB966, 100% of displacement was due to conformational change (Figure 3I), and displacement corresponded exactly to the distance between adjacent peaks of the bacterial sine wave (2.83 μm) (Goldstein et al., 1996). By contrast, GCB971 displacement during each interaction was greater than one wavelength, and conformational change did not account for all of this strain's displacement (Figures 3I and 3J). These data implied that BBK32-dependent adhesion complexes were stationary and maintained the same position relative to the endothelium as bacteria rotated. However, BBK32-independent complexes slid past the initial adhesion site, possibly by retrograde dragging of the adhesion complex along the bacterial membrane, or upon extension of tethers (see below).

Collectively, these data implied that *B. burgdorferi* moved via a series of stepwise rotations, which oriented adhesion sites at successive sine-wave peaks toward endothelial surfaces (Figure 3K). This mechanism resembled the rotation-dependent surface adhesion strategies of motile *Vibrio cholerae* and *Caulobacter crescentus* under flow, in which cell body rotation in response to flagellar rotation (*V. cholerae*) or torque due to flow (*C. crescentus*) orients adhesive pili closer to attachment surfaces (Persat et al., 2014; Utada et al., 2014). For *B. burgdorferi*, this rotation could have been passively driven by torque due to flow and possibly by active rotation of periplasmic flagella, since the forces experienced by these bacteria under flow were generally smaller than bacterial propulsive force generated by motility (see below).

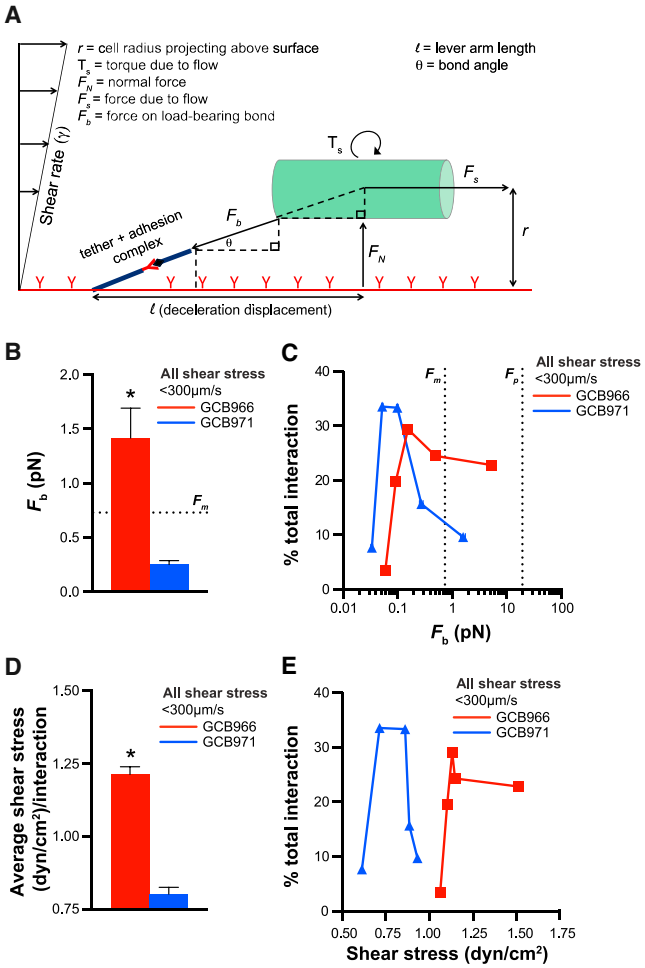


**Figure 4. Forces Experienced by *B. burgdorferi* Interacting with Endothelia under Flow**

(A) Schematic: forces and parameters affecting adhesion of *B. burgdorferi* (shown as a cylinder) to endothelial surfaces under flow.

(B–E) Average bond forces ($F_b$) (B) and shear stresses (D) for all interactions. Percentages of total interactions occurring at indicated $F_b$ (C) and shear stress (E) values. In (C) and (E), x axis values are mean $F_b$ and shear stress values for interactions binned by bacterial length. The estimated *B. burgdorferi* propulsive force generated by bacterial motility (B and C: $F_m$) is greater than or equal to average bond forces for most interactions. *B. burgdorferi* bond forces are less than the force at which receptors unanchored to cytoskeletal structures are plucked from lipid bilayers (C: $F_p$). BBK32-producing GCB966 adhere to endothelia at higher bond forces and shear stresses (*$p < 0.05$) than the *bbk32*-null GCB966 derivative GCB971.

See also Figure S4.

## Bacteria Experience Less Force and Torque during Endothelial Interactions under PCV Shear Stress Conditions than Rolling Leukocytes

To understand the mechanisms mediating bacterial-endothelial interactions under flow, it was essential to investigate the forces involved in these interactions (Figures 4A and S4A). Objects adhering to surfaces under flow are subjected to force exerted parallel to flow ($F_s$) and rotational torque ($T_s$), which peels cells from surfaces (Figures 4A and S4A) (Sundd et al., 2011). $F_s$ and $T_s$ increase exponentially as cells project higher above surfaces (Figure S4A). As a result, *B. burgdorferi* adhering to endothelia experienced the greatest $F_s$ and $T_s$ at interaction outset (Figures S4B and S4C) when they projected highest above surfaces (Figures 3G and 3H), and BBK32-producing GCB966 was subjected to larger $F_s$ and $T_s$ than *bbk32*-deficient GCB971 (Figures S4D and S4E). Average $F_s$ and $T_s$ experienced by bacteria were at least 10 times smaller than $F_s$ and $T_s$ experienced by rolling leukocytes at similar shear stresses (Sundd et al., 2011), due to the relatively small *B. burgdorferi* radius. Therefore, counterintuitively, the small size of bacteria made them less sensitive to force and torque imposed by flow than leukocytes. Since most bacteria are as small or smaller than *B. burgdorferi*, this conclusion is likely to be true for other bacteria.

## Forces Imposed on *B. burgdorferi* Load-Bearing Bonds during Most Interactions Are Smaller Than the Estimated Propulsive Force of Bacterial Motility

Cells adhering to surfaces under flow experience $F_s$ as the force imposed on their load-bearing bonds ($F_b$). The force loaded on these bonds is a function of $F_s$ and bond angle, which can be estimated from the height cells project above surfaces and the distance they displace during each interaction (Figures 4A, S4A, and S4F–S4H) (Sundd et al., 2011). Larger interaction bond angles were more frequently observed for BBK32-producing GCB966 than *bbk32*-deficient GCB971 interactions because BBK32-expressing bacteria were more likely to project higher above endothelial surfaces and displaced shorter distances (Figure S4I).

It was especially important to estimate bond forces during *B. burgdorferi* interactions because this bacterium's adhesins are located in its outer membrane and not on force-distributing structures such as flagella, pili, or fimbriae (Bergström and Zückert, 2010) and because proteins in lipid bilayers that are not anchored to such structures are plucked from membranes at low forces (~20 pN) (Evans et al., 1991). Thus, we expected that bond forces for adhesion complexes mediating *B. burgdorferi* interactions would likely be smaller than the force at which unanchored adhesins are plucked from membranes. Indeed, average estimated bond forces for GCB966 and GCB971 were <20 pN (Figure 4B). Surprisingly, we also found that average bond forces (Figure 4B) and forces imposed on bacteria by flow (Figure S4E) were similar to or smaller than the predicted propulsive force generated by bacterial motility ($F_m$: ~0.72 pN; Figure S4) (Wolgemuth, 2008), as were the bond forces of most interactions (Figure 4C). Thus, unexpectedly, *B. burgdorferi* experienced forces that were small enough to be overcome by bacterial motility. This finding suggested that motility is possibly strong enough to modulate the force imposed on load-bearing bonds and drive active bacterial migration over endothelia under PCV shear stress.

## BBK32 Expression Increases the Force Sustained by Load-Bearing Bonds and the Shear Stress Range of *B. burgdorferi*-Endothelial Interactions

We also found that average bond forces for BBK32-producing GCB966 were larger than for *bbk32*-deficient GCB971 (Figure 4B), that most GCB966 interactions occurred at higher bond forces than GCB971 (Figure 4C), and that GCB966 interactions occurred at a higher average shear stress and shear stress

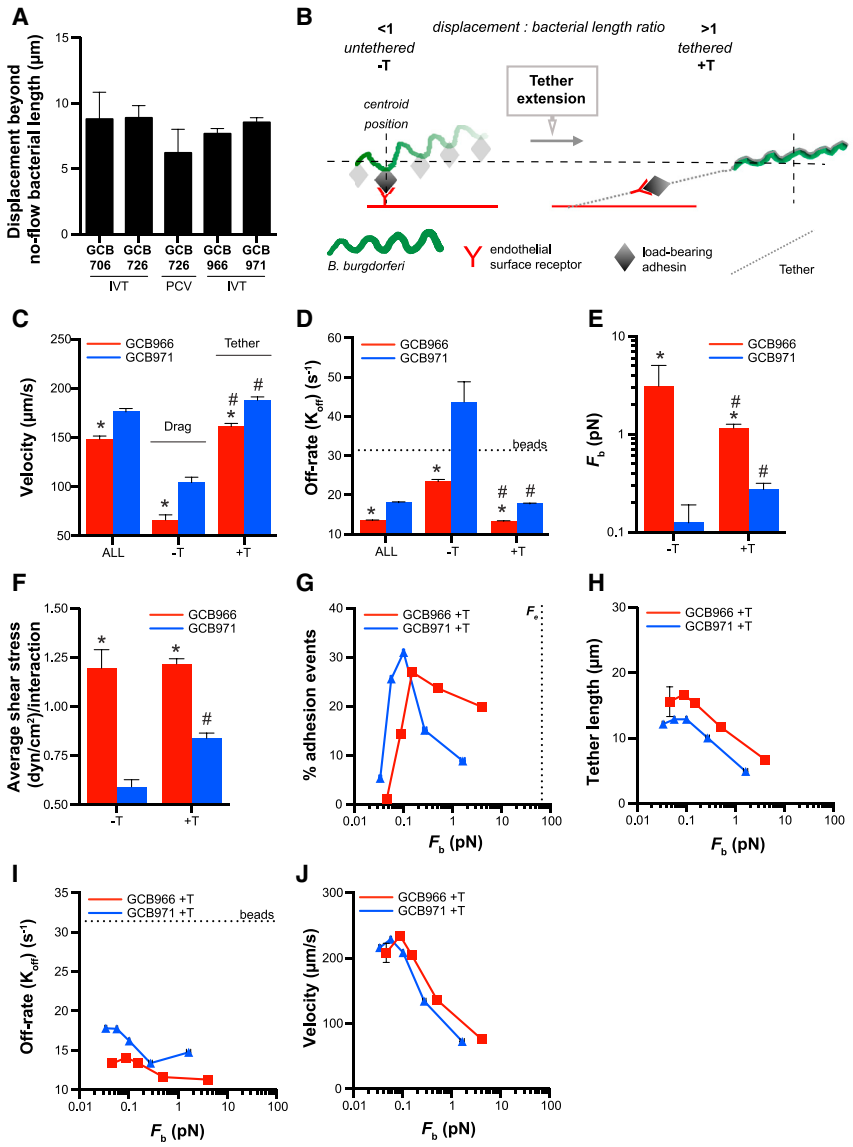


**Figure 5. Interaction Stabilization by Tethers**

(A) Average distance bacteria displace beyond their average cell length during endothelial interactions under flow, suggesting that bacteria are anchored to endothelia by tethers.

(B) Schematic: method for distinguishing untethered (–T) and tethered (+T) interactions, based on ratios of displacement: bacterial length under flow (ratios of <1 and >1 for –T and +T interactions, respectively).

(C–F) Velocities (C), dissociation rates (D), bond forces (E), and shear stresses (F) of –T and +T interactions and all interactions combined (ALL). Average –T and +T velocities (C) (< and >100 μm/s, respectively) correspond to velocities of mechanistically distinct tethering and dragging interaction types previously described in PCVs. Tethering stabilizes (D) and increases interaction bond force (E) and shear stress (F), especially for BBK32-deficient bacteria.

(G–J) Percentage of total interactions (G), tether lengths (H), dissociation rates (I), and velocities (J) for +T interactions at indicated bond forces. Tethers shorten (H) and +T interactions dissociate more slowly (I) with increasing bond force for both GCB966 and GCB971 (up to ~0.25 pN), suggesting that tethers stabilize adhesion by a BBK32-independent catch bond mechanism and/or become stiffer with increasing force. Tethering occurs at smaller bond forces than the force required to pull membranous tethers from endothelia (G: $F_e$).

Beads (D and I): threshold at which interactions dissociate as fast as non-adherent beads, i.e., are unstable. *$p < 0.05$ versus GCB966 within –T and +T groups, #$p < 0.05$ –T versus +T intra-strain. Bacterial strains: adhesion-attenuated *bbk32*-null GCB706, adhesive BBK32-expressing GCB726 and GCB966, *bbk32*-null GCB966-derived GCB971. See also Figure S5.

range than GCB971 interactions (Figures 4D and 4E). These differences between GCB966 and GCB971 bond force and shear stress ranges were not trivial. Linear increases in shear stress over the range that is typical in PCVs cause exponential increases in bond breakage and cell detachment from surfaces if adhesion complexes are not stabilized by mechanisms such as catch bonds and tethers (Park et al., 2002; Sundd et al., 2011). Thus, the ability of BBK32 to mediate adhesion at higher bond forces and shear stresses likely extends the shear stress range at which bacterial interactions can occur in PCVs, a property that could contribute to this adhesin's importance for early tissue dissemination (Hyde et al., 2011).

## Interaction Stabilization by Tethers Anchoring Bacteria to Endothelia

Since conventional slip bonds are not stable over the PCV shear stress range (Park et al., 2002), interactions in these vessels are typically stabilized by mechanisms such as catch bonds and tethers, which increase bond lifetime and confer tensile strength under increasing force (Sundd et al., 2011). Tethers are bond-associated structures somewhat analogous to bungee cords, which increase bond stability by absorbing/distributing force (Ramachandran et al., 2004; Sundd et al., 2011). Tethers anchoring rolling leukocytes are derived from leukocyte and endothelial membranes and can be as long as 20 μm (Girdhar and Shao, 2004).

We noted that all bacterial strains interacting with endothelia in flow chambers and PCVs typically displaced ~5–10 μm longer than their cell length under static conditions (Figure 5A). This suggested the possibility that, like leukocytes, bacteria were anchored to endothelia by tethers. As described in Figures S5A–S5F, we determined that sorting interactions into two groups based on the ratio of each bacterium's displacement to its cell length under flow identified two interaction populations with distinct physical properties. As summarized schematically in Figure 5B, one population displaced less than bacterial length during each interaction (ratio <1). We referred to this interaction

group as untethered (–T). The second population displaced further than bacterial length (ratio >1). We referred to this interaction group as tethered (+T).

–T and +T interactions exhibited distinct velocities (Figure 5C), and classifying interactions into –T and +T groups accurately distinguished the two mechanistically distinct types of transient *B. burgdorferi* interactions previously identified in PCVs, dragging and tethering (Moriarty et al., 2008; Norman et al., 2008). –T interaction velocities were <100 μm/s (Figure 5C), corresponding to the velocity of dragging interactions (Moriarty et al., 2008). +T interaction velocities were >100 μm/s (Figure 5C), similar to tethering interaction velocities (Moriarty et al., 2008). Moreover, –T and +T interactions comprised ~15% and 85% of total interactions, respectively (Figure S5H), similar to the percentage of interactions that drag and tether in PCVs (~10% and 90%, respectively) (Moriarty et al., 2008, 2012). Thus, sorting interactions by displacement: bacterial length ratios accurately discriminated between dragging and tethering.

Tethers prolong the lifetime of load-bearing bonds by reducing and/or distributing the force imposed on them (Sundd et al., 2011). To determine whether interactions where bacteria displaced further than their length under flow exhibited properties associated with anchoring by tethers, we compared dissociation rates and bond forces for –T and +T interactions (Figures 5D and 5E), as well as the average shear stress at which these interactions occurred (Figure 5F).

Despite their faster velocity +T interactions dissociated more slowly than –T interactions (Figure 5D), indicating that they were more stable. Average bond force and shear stress were also greater for +T than –T interactions for the *bbk32* mutant GCB971, but not for BBK32-producing GCB966 (Figures 5E and 5F). These data showed that +T interactions exhibited hallmark properties of tether-anchored interactions and suggested that tethering extended the bond force and shear stress range at which interactions could occur in the absence of BBK32.

Although average bond force and shear stress were higher for +T GCB966 than +T GCB971 interactions (Figures 5E and 5F), and tethering did not occur for BBK32-dependent interactions until a larger bond force (Figure 5G), the physical properties of GCB966 and GCB971 +T interactions were surprisingly similar. For both strains, tether length decreased (Figure 5H) as bond lifetime increased (Figure 5I), and velocity changes in +T interactions with increasing bond force (Figure 5J) and shear stress (Figure S5I) were strikingly similar. This suggested that GCB966 and GCB971 tethering mechanisms were the same. These data also indicated that tethers exhibited catch bond properties, since bond lifetime increased as force increased (Figure 5I) (Sokurenko et al., 2008).

It also appeared that tethers were formed by materials or structures with non-linear elastic properties that stiffened with increasing force, since tether length decreased as force increased (Figure 5H) (Wen and Janmey, 2013). It was unlikely that endothelial membranes formed these tethers, since membrane tethers exhibit yielding elastic properties and are extended at a much higher force than *B. burgdorferi* bond forces (~55 pN) (Beaussart et al., 2014; Chen et al., 2010; Whitfield et al., 2014). It is possible that tethers were formed by mechanically responsive biopolymers such as Fn (Chabria et al., 2010; Deravi et al., 2012; Früh et al., 2015), which is a key mediator of *B. burgdorferi* tethering interactions in PCVs (Moriarty et al., 2012; Norman et al., 2008). Together, these data suggested that *B. burgdorferi*-endothelial associations were stabilized by non-membranous tethers with non-linear elastic properties.

## Interaction Stabilization by a BBK32-Dependent Catch Bond Mechanism

Given that BBK32-producing GCB966 bacteria dissociated more slowly than *bbk32*-deficient GCB971 at higher bond forces and shear stresses (Figures 5D–5F), we also asked whether BBK32 stabilized adhesion by a catch bond mechanism. Catch bonds are force-strengthened bonds that stabilize (become longer lived) at forces higher than a specific activation threshold; they mediate diverse biological processes subject to tension, stabilize cell-cell interactions in force-variable environments, permit cells to discriminate between surface-anchored and soluble molecules, and act as force sensors regulating homing to specific environments (Sokurenko et al., 2008). These properties would likely be crucial for disseminating bacteria. However, adhesins conferring catch bond properties to bacterial-endothelial interactions under vascular shear stress have not been identified.

To determine whether BBK32 conferred catch bond properties to interactions, we examined changes in dissociation rates with increasing bond force for interactions. Since tethers stabilized interactions (slowed dissociation rates), we performed this analysis only for untethered (–T) interactions, to eliminate potential confounding effects of tether-dependent stabilization. Untethered BBK32-deficient GCB971 interactions dissociated rapidly at ~0.6 dyn/cm$^2$ (Figure 6A) and 0.08 pN (Figure 6B) and accounted for fewer than 1% of total interactions at shear stresses and bond forces above these values (Figures 6C and 6D), where interaction numbers were insufficient for dissociation rate measurement. This implied that untethered BBK32-independent adhesion was unstable at forces $\geq$0.08 pN.

By contrast, BBK32-producing GCB966 interactions were stable up to 0.08 pN, dissociated more quickly as force rose from ~0.1–0.25 pN, and then became increasingly longer lived at forces >0.25 pN, up to the force threshold at which unanchored adhesion complexes are plucked from membranes (~20 pN; Figure 6B) (Evans et al., 1991). GCB966 interaction velocity also progressively decreased with increasing force above 0.25 pN (Figure 6E), indicating that bacteria moved more slowly as bonds stabilized. Thus, BBK32 stabilized interactions by a catch bond mechanism, whereas BBK32-independent interactions exhibited conventional slip bond properties (Figure 6F), which are stable only over narrow force ranges and break at exponential rates with linear force increases (Park et al., 2002).

BBK32-dependent catch bond properties were also observed for tethered interactions at bond forces above 0.25 pN, where GCB966 dissociation rates slowed while GCB971 rapidly dissociated (Figure 5I). This implied that BBK32 catch bond properties could stabilize both tethered and untethered *B. burgdorferi*-endothelial interactions. The BBK32 catch bond force regime ranged from ~2 to 19 pN and was similar to the catch bond force regimes of selectins (~5–50 pN), which are the major molecular mediators of leukocyte rolling at the PCV shear stress range (Marshall et al., 2003; Sarangapani et al., 2004).

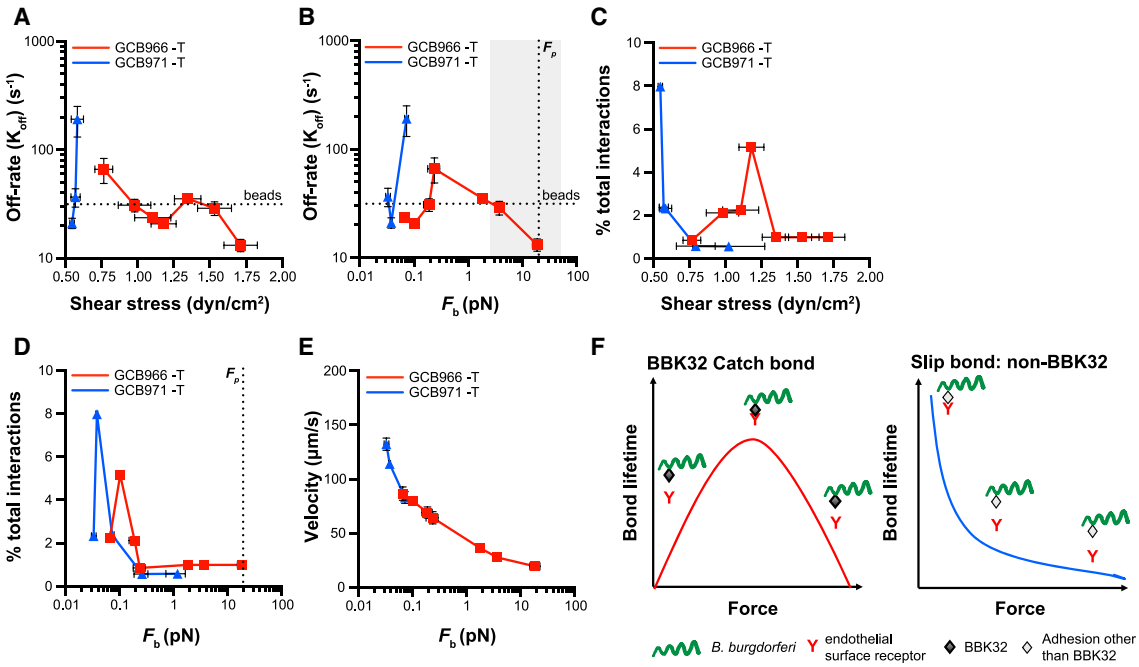


**Figure 6. Interaction Stabilization by BBK32-Dependent Catch Bond Mechanism**

In the absence of tether-dependent stabilization, untethered (–T) interactions are strengthened by a BBK32-dependent catch bond mechanism.

(A–E) Dissociation rates (A and B), percentage of total interactions (C and D), and velocities (E) at indicated shear stresses (A and C) and bond forces (B, D, and E). Above an activation threshold of ~0.25 pN, BBK32-dependent bonds become progressively longer lived with increasing force—i.e., are stabilized by a catch bond mechanism, up to the force at which proteins unanchored to cytoskeletal structures are plucked from membranes (B: $F_p$). Leukocyte selectin (gray shading) and BBK32 catch bond force regimes overlap (B). Threshold at which interactions dissociate as fast as non-adherent beads: "beads."

(F) Schematic illustrating catch bond behavior of BBK32-dependent interactions and slip bond behavior of BBK32-independent interactions.

Strains: *bbk32*-expressing and -null GCB966 and GCB971.

Although these data showed that BBK32 stabilizes *B. burgdorferi*-endothelial interactions and extends the force and shear stress range at which they occur by a catch bond mechanism, many questions remain. BBK32 is a multi-functional protein containing both lectin (GAG-binding) and Fn-binding sequences, which contribute to both tethering and dragging interactions in PCVs (Lin et al., 2015; Moriarty et al., 2012). Lectin domains play key roles in several catch bond mechanisms, and Fn forms catch bonds with integrin $\alpha_5\beta_1$ (Kong et al., 2009; Le Trong et al., 2010; Waldron and Springer, 2009). Thus, multiple BBK32 ligand-binding sites could potentially form or reciprocally regulate catch bond formation. Equally, catch bonds could be formed by BBK32 host ligands, and not by BBK32 itself. Finally, BBK32's Fn-binding sequences interact with a mechanosensitive Fn epitope, induce Fn conformational extension and aggregation, and bind to Fn by the same mechanism as Fn-binding proteins from evolutionarily distant Gram-positive pathogens (Chabria et al., 2010; Harris et al., 2014; Kim et al., 2004; Prabhakaran et al., 2009). Thus, it is possible that BBK32 binding may confer novel biomechanical properties to host target molecules and that BBK32-like catch bond properties may be functionally conserved in adhesins of other pathogens.

## Conclusions

These studies show that, despite striking differences in phylogeny, form, and function, the physical mechanisms supporting *B. burgdorferi* and leukocyte interactions with endothelia under shear stress are remarkably conserved (Figure 7). We propose that catch bonds and tethering are common cellular responses to the universal problem of vascular adhesion under shear stress and likely facilitate dissemination of other extracellular pathogens.

## EXPERIMENTAL PROCEDURES

Detailed methods are provided in the Supplemental Experimental Procedures.

### Ethics Statement

This study was carried out in compliance with Canadian Council on Animal Care guidelines, under University of Toronto protocols 20009347, 20009908, and 20010430.

### Flow Chamber Experiments

Primary human endothelia purchased from Lonza were cultivated according to supplier recommendations, seeded at $1.6 \times 10^5$ cells/channel of ibiTreat Ibidi μ-Slides VI$^{0.4}$ (Ibidi), cultured to 2 days post-confluence, and labeled with CellMask Deep Red dye (Life Technologies) 5 min before imaging. *B. burgdorferi* were resuspended to $1 \times 10^8$/ml in HBSS (Life Technologies) containing 10% FBS and perfused over endothelia in flow chambers mounted in a stage-top incubator, using a syringe pump.

### Intravital Microscopy

As described (Moriarty et al., 2012), IVM was performed in PCVs of flank skin of 5- to 6-week-old male C57BL/6 mice (Charles River Laboratories)

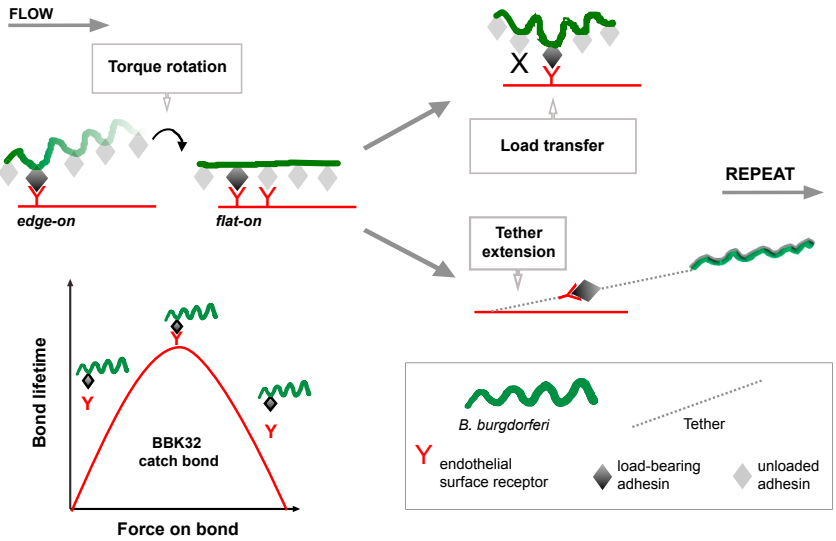


**Figure 7. Model: Biomechanics of *B. burgdorferi*-Endothelial Interactions under Physiological Shear Stress**

At the PCV shear stress range, *B. burgdorferi* move over endothelia by stepwise rotations driven by torque due to flow and possibly bacterial motility. Bacterial rotation presents adhesins at bacterial sine-wave peaks to endothelial receptors, facilitating transfer of mechanical load from peak to peak along series of single or coordinated, tightly clustered adhesion complexes. This process is stabilized by tethers anchoring bacteria to endothelia that become shorter and longer lived with increasing force and are strengthened by but do not require BBK32. BBK32 extends the interaction force and shear stress range by a catch bond mechanism.

anesthetized with 10 mg/kg xylazine (MTC Pharmaceuticals) and 200 mg/kg ketamine hydrochloride (Rogar/STB), after intravenous tail vein injection of $4 \times 10^8$ bacteria.

### Time-Lapse Imaging and Analysis

Flow chamber and IVM time lapses were acquired at 15 fps by spinning disk confocal microscopy using Volocity software (Improvision/Perkin-Elmer). *B. burgdorferi* tethering and dragging were counted as described (Moriarty et al., 2008) in 100-μm-long unbranched PCVs and in a 30 × 100-μm region at the center of flow chamber channels. Centroid-based tracking of individual bacteria was performed in Volocity. Tracking procedures and formulas used to analyze tracks are described in figures, supplemental figures, and in the Supplemental Experimental Procedures.

### Statistical Analysis

Statistical analysis was performed in GraphPad Prism (GraphPad). Specific tests used are noted in figure legends.

## SUPPLEMENTAL INFORMATION

Supplemental Information includes Supplemental Experimental Procedures, five figures, two tables, and four movies and can be found with this article online at http://dx.doi.org/10.1016/j.celrep.2016.08.013.

## AUTHOR CONTRIBUTIONS

Conceptualization, R.E. and T.J.M.; Methodology, R.E., A.F.N., N.G., T.T.T., and T.J.M.; Software, R.E., N.G., and T.J.M.; Validation, R.E., A.F.N., C.A.S., J.T.S., and T.J.M.; Formal Analysis, R.E., A.B., C.A.S., and T.J.M.; Investigation, R.E., A.F.N., A.E.B., Y.R.K., T.T.T., T.O., H.Z., and T.J.M.; Resources, J.T.S. and T.J.M.; Data Curation, R.E. and T.J.M.; Writing – Original Draft, R.E., T.O., and T.J.M.; Review and Editing, R.E., A.F.N., A.E.B., Y.R.K., T.T.T., N.G., H.Z., C.A.S., J.T.S., and T.J.M.; Visualization, R.E., T.O., and T.J.M.; Supervision, J.T.S. and T.J.M.; Project Administration, T.J.M.; Funding Acquisition, J.T.S. and T.J.M.

## ACKNOWLEDGMENTS

Manuscript review: C. Cameron, G. Chaconas, P. de Figueiredo, M. Glogauer, Y.P. Lin, C. McCulloch, H. Mohammadi, C. Wolgemuth, and T.J.M.'s lab members. Writing support: F. Thong. BBK32 antibody: S. Meri. Bacterial strains: G. Chaconas. Technical support: A. Bansal, A. Javid, C. Lo, DCM, and Sick Kids Imaging Facility. Funding: T.J.M.: CIHR (MOP-11959, ICS-12398), NSERC (RGPIN 401), Banting Research Foundation, CFI/ORF (27881); J.T.S.: NIH (PHSG AI058086, AI119821), UofT (R.E., A.F.N., A.E.B., N.G., and T.T.T.) and Harron (R.E., A.F.N., and A.E.B.) Fellowships; OGS (R.E.), QEII (T.T.T.), CIHR IMHA (N.G.), and NSERC USRA (T.T.T.) scholarships.

Received: April 1, 2016
Revised: July 21, 2016
Accepted: August 2, 2016
Published: August 25, 2016

## REFERENCES

Alon, R., Hammer, D.A., and Springer, T.A. (1995). Lifetime of the P-selectin-carbohydrate bond and its response to tensile force in hydrodynamic flow. Nature *374*, 539–542.

Alon, R., Chen, S., Puri, K.D., Finger, E.B., and Springer, T.A. (1997). The kinetics of L-selectin tethers and the mechanics of selectin-mediated rolling. J. Cell Biol. *138*, 1169–1180.

Beaussart, A., Baker, A.E., Kuchma, S.L., El-Kirat-Chatel, S., O'Toole, G.A., and Dufrêne, Y.F. (2014). Nanoscale adhesion forces of *Pseudomonas aeruginosa* type IV Pili. ACS Nano *8*, 10723–10733.

Bergström, S., and Zückert, W.R. (2010). Structure, function and biogenesis of the *Borrelia* cell envelope. In *Borrelia*: Molecular Biology, Host Interaction, and Pathogenesis, D.S. Samuels and J.D. Radolf, eds. (Caister Academic Press), pp. 139–166.

Chabria, M., Hertig, S., Smith, M.L., and Vogel, V. (2010). Stretching fibronectin fibres disrupts binding of bacterial adhesins by physically destroying an epitope. Nat. Commun. *1*, 135.

Charon, N.W., Cockburn, A., Li, C., Liu, J., Miller, K.A., Miller, M.R., Motaleb, M.A., and Wolgemuth, C.W. (2012). The unique paradigm of spirochete motility and chemotaxis. Annu. Rev. Microbiol. *66*, 349–370.

Chen, Y., Yao, D.-K., and Shao, J.-Y. (2010). The constitutive equation for membrane tether extraction. Ann. Biomed. Eng. *38*, 3756–3765.

Claes, J., Vanassche, T., Peetermans, M., Liesenborghs, L., Vandenbriele, C., Vanhoorelbeke, K., Missiakas, D., Schneewind, O., Hoylaerts, M.F., Heying, R., and Verhamme, P. (2014). Adhesion of *Staphylococcus aureus* to the vessel wall under flow is mediated by von Willebrand factor-binding protein. Blood *124*, 1669–1676.

Deravi, L.F., Su, T., Paten, J.A., Ruberti, J.W., Bertoldi, K., and Parker, K.K. (2012). Differential contributions of conformation extension and domain unfolding to properties of fibronectin nanotextiles. Nano Lett. *12*, 5587–5592.

Please cite this article in press as: Ebady et al., Biomechanics of *Borrelia burgdorferi* Vascular Interactions, Cell Reports (2016), http://dx.doi.org/10.1016/j.celrep.2016.08.013

Evans, E., Berk, D., and Leung, A. (1991). Detachment of agglutinin-bonded red blood cells. I. Forces to rupture molecular-point attachments. Biophys. J. *59*, 838–848.

Fiore, V.F., Ju, L., Chen, Y., Zhu, C., and Barker, T.H. (2014). Dynamic catch of a Thy-1-$\alpha_5\beta_1$+syndecan-4 trimolecular complex. Nat. Commun. *5*, 4886.

Früh, S.M., Schoen, I., Ries, J., and Vogel, V. (2015). Molecular architecture of native fibronectin fibrils. Nat. Commun. *6*, 7275.

Girdhar, G., and Shao, J.-Y. (2004). Membrane tether extraction from human umbilical vein endothelial cells and its implication in leukocyte rolling. Biophys. J. *87*, 3561–3568.

Goldstein, S.F., Buttle, K.F., and Charon, N.W. (1996). Structural analysis of the *Leptospiraceae* and *Borrelia burgdorferi* by high-voltage electron microscopy. J. Bacteriol. *178*, 6539–6545.

Harris, G., Ma, W., Maurer, L.M., Potts, J.R., and Mosher, D.F. (2014). *Borrelia burgdorferi* protein BBK32 binds to soluble fibronectin via the N-terminal 70-kDa region, causing fibronectin to undergo conformational extension. J. Biol. Chem. *289*, 22490–22499.

Hyde, J.A., Weening, E.H., Chang, M., Trzeciakowski, J.P., Höök, M., Cirillo, J.D., and Skare, J.T. (2011). Bioluminescent imaging of *Borrelia burgdorferi in vivo* demonstrates that the fibronectin-binding protein BBK32 is required for optimal infectivity. Mol. Microbiol. *82*, 99–113.

Kim, J.H., Singvall, J., Schwarz-Linek, U., Johnson, B.J., Potts, J.R., and Höök, M. (2004). BBK32, a fibronectin binding MSCRAMM from *Borrelia burgdorferi*, contains a disordered region that undergoes a conformational change on ligand binding. J. Biol. Chem. *279*, 41706–41714.

Kim, J., Zhang, C.-Z., Zhang, X., and Springer, T.A. (2010). A mechanically stabilized receptor-ligand flex-bond important in the vasculature. Nature *466*, 992–995.

Kong, F., García, A.J., Mould, A.P., Humphries, M.J., and Zhu, C. (2009). Demonstration of catch bonds between an integrin and its ligand. J. Cell Biol. *185*, 1275–1284.

Le Trong, I., Aprikian, P., Kidd, B.A., Forero-Shelton, M., Tchesnokova, V., Rajagopal, P., Rodriguez, V., Interlandi, G., Klevit, R., Vogel, V., et al. (2010). Structural basis for mechanical force regulation of the adhesin FimH via finger trap-like beta sheet twisting. Cell *141*, 645–655.

Lemichez, E., Lecuit, M., Nassif, X., and Bourdoulous, S. (2010). Breaking the wall: targeting of the endothelium by pathogenic bacteria. Nat. Rev. Microbiol. *8*, 93–104.

Lin, Y.-P., Chen, Q., Ritchie, J.A., Dufour, N.P., Fischer, J.R., Coburn, J., and Leong, J.M. (2015). Glycosaminoglycan binding by *Borrelia burgdorferi* adhesin BBK32 specifically and uniquely promotes joint colonization. Cell. Microbiol. *17*, 860–875.

Mairey, E., Genovesio, A., Donnadieu, E., Bernard, C., Jaubert, F., Pinard, E., Seylaz, J., Olivo-Marin, J.-C., Nassif, X., and Duménil, G. (2006). Cerebral microcirculation shear stress levels determine *Neisseria meningitidis* attachment sites along the blood-brain barrier. J. Exp. Med. *203*, 1939–1950.

Marshall, B.T., Long, M., Piper, J.W., Yago, T., McEver, R.P., and Zhu, C. (2003). Direct observation of catch bonds involving cell-adhesion molecules. Nature *423*, 190–193.

Mikaty, G., Soyer, M., Mairey, E., Henry, N., Dyer, D., Forest, K.T., Morand, P., Guadagnini, S., Prévost, M.C., Nassif, X., and Duménil, G. (2009). Extracellular bacterial pathogen induces host cell surface reorganization to resist shear stress. PLoS Pathog. *5*, e1000314.

Moriarty, T.J., Norman, M.U., Colarusso, P., Bankhead, T., Kubes, P., and Chaconas, G. (2008). Real-time high resolution 3D imaging of the lyme disease spirochete adhering to and escaping from the vasculature of a living host. PLoS Pathog. *4*, e1000090.

Moriarty, T.J., Shi, M., Lin, Y.-P., Ebady, R., Zhou, H., Odisho, T., Hardy, P.-O., Salman-Dilgimen, A., Wu, J., Weening, E.H., et al. (2012). Vascular binding of a pathogen under shear force through mechanistically distinct sequential interactions with host macromolecules. Mol. Microbiol. *86*, 1116–1131.

Norman, M.U., Moriarty, T.J., Dresser, A.R., Millen, B., Kubes, P., and Chaconas, G. (2008). Molecular mechanisms involved in vascular interactions of the Lyme disease pathogen in a living host. PLoS Pathog. *4*, e1000169.

Park, E.Y.H., Smith, M.J., Stropp, E.S., Snapp, K.R., DiVietro, J.A., Walker, W.F., Schmidtke, D.W., Diamond, S.L., and Lawrence, M.B. (2002). Comparison of PSGL-1 microbead and neutrophil rolling: microvillus elongation stabilizes P-selectin bond clusters. Biophys. J. *82*, 1835–1847.

Persat, A., Stone, H.A., and Gitai, Z. (2014). The curved shape of *Caulobacter crescentus* enhances surface colonization in flow. Nat. Commun. *5*, 3824.

Persat, A., Nadell, C.D., Kim, M.K., Ingremeau, F., Siryaporn, A., Drescher, K., Wingreen, N.S., Bassler, B.L., Gitai, Z., and Stone, H.A. (2015). The mechanical world of bacteria. Cell *161*, 988–997.

Prabhakaran, S., Liang, X., Skare, J.T., Potts, J.R., and Höök, M. (2009). A novel fibronectin binding motif in MSCRAMMs targets F3 modules. PLoS ONE *4*, e5412.

Ramachandran, V., Williams, M., Yago, T., Schmidtke, D.W., and McEver, R.P. (2004). Dynamic alterations of membrane tethers stabilize leukocyte rolling on P-selectin. Proc. Natl. Acad. Sci. USA *101*, 13519–13524.

Sarangapani, K.K., Yago, T., Klopocki, A.G., Lawrence, M.B., Fieger, C.B., Rosen, S.D., McEver, R.P., and Zhu, C. (2004). Low force decelerates L-selectin dissociation from P-selectin glycoprotein ligand-1 and endoglycan. J. Biol. Chem. *279*, 2291–2298.

Seshu, J., Esteve-Gassent, M.D., Labandeira-Rey, M., Kim, J.H., Trzeciakowski, J.P., Höök, M., and Skare, J.T. (2006). Inactivation of the fibronectin-binding adhesin gene *bbk32* significantly attenuates the infectivity potential of *Borrelia burgdorferi*. Mol. Microbiol. *59*, 1591–1601.

Sokurenko, E.V., Vogel, V., and Thomas, W.E. (2008). Catch-bond mechanism of force-enhanced adhesion: counterintuitive, elusive, but … widespread? Cell Host Microbe *4*, 314–323.

Sundd, P., Pospieszalska, M.K., Cheung, L.S.-L., Konstantopoulos, K., and Ley, K. (2011). Biomechanics of leukocyte rolling. Biorheology *48*, 1–35.

Utada, A.S., Bennett, R.R., Fong, J.C.N., Gibiansky, M.L., Yildiz, F.H., Golestanian, R., and Wong, G.C.L. (2014). *Vibrio cholerae* use pili and flagella synergistically to effect motility switching and conditional surface attachment. Nat. Commun. *5*, 4913.

Waldron, T.T., and Springer, T.A. (2009). Transmission of allostery through the lectin domain in selectin-mediated cell adhesion. Proc. Natl. Acad. Sci. USA *106*, 85–90.

Wen, Q., and Janmey, P.A. (2013). Effects of non-linearity on cell-ECM interactions. Exp. Cell Res. *319*, 2481–2489.

Whitfield, M.J., Luo, J.P., and Thomas, W.E. (2014). Yielding elastic tethers stabilize robust cell adhesion. PLoS Comput. Biol. *10*, e1003971.

Wolgemuth, C.W. (2008). Collective swimming and the dynamics of bacterial turbulence. Biophys. J. *95*, 1564–1574.

Wormser, G.P. (2006). Dissemination and persistence are pathogenic events common to all of the major human spirochetal infections. In Molecular Biology of Spirochetes (IOS Press), pp. 3–10.